IJCRT.ORG ISSN : 2320-2882

INTERNATIONAL JOURNAL OF CREATIVE RESEARCH THOUGHTS (IJCRT)

An International Open Access, Peer-reviewed, Refereed Journal

An Experimental Cum Mathematical study on Lattice Dynamics

Er. Birendra Jha[1]

[1]Senior Lecturer, Government Polytechnic, Siwan, Bihar

Abstract

Lattice Dynamics the concept of a phonon and its properties were first introduced by Debye [3] in 1912. A phonon is defined as a quantum of vibrational energy within a crystal structure. Phonons are considered as a quasi-particle with wave vector q and angular frequency ω_s for atomic vibrational polarization s. The energy of a phonon mode is $h\omega_s$ and its momentum is h q. Lattice dynamics is the study of the relationship between these two quantities: $\omega = \omega s(q)$. In the present study an experimental cum mathematical modeling was performed to study how phonon dispersion curves arise. The continuum model has been employed to explain the phonon dispersion of semiconducting nanostructures. The result shows that for the silicon nanostructures, the ultra-small case of each structure that all branches except the acoustic are flat and dispersion less regardless of whether the system is zero-, one-or two-dimensional. Conversely, the continuum model of the nanotube shows that the group velocity of the low optical modes is much large for k > 1. As the size of the silicon structures increases, these branches are seen to become dispersive in the direction of propagation like the nanotube.

Keywords: Lattice dynamics; quantum; structure; model; nanotube.

1. Introduction

To understand how phonon dispersion curves, arise, one must first understand the crystal potential and define the atomic co-ordinates [1]. The atomic co-ordinates of a system are defined using the unit cell vector 1, and the relative position, b, of the atom within this unit cell [2-4]. This is the mean position or the equilibrium position of the atom. In reality the bth atom will be located at position r (1b) at time t as it will be vibrating. Hence the displacement, u (1b), of atom lb may be written as

$$u(lb) = r(lb) - (1+b)$$

$$u(lb) = r(lb) - x(lb), \qquad (1)$$

where x (lb) = (l + b).

1.1 The Development of Lattice Dynamics

The last century has seen the proposal and development of several models to describe the lattice dynamics of covalently bonded materials [5-7]. These models vary greatly in complexity from simple continuum models to detailed ab initio models. Each of these models have different uses and applications in various areas. The field of lattice dynamics began to take form in 1912 when Debye proposed a simple model known as the elastic isotropic continuum model [8-9]. In this model the atomic crystal structure was smeared out and treated as a continuous elastic medium. This is the easiest and most simplistic view of a solid semiconductor that may be taken when discussing its vibrational behavior. It is surprisingly effective for such a simple model and can form a basis in estimating the basic thermal feature of a semiconductor. By applying this model, it is possible to relate the elastic constants that describe the semiconductor to the zone-centre group velocities Cs of an acoustic phonon mode ωs(q). The dispersion relation Debye obtained for the frequency of a phonon mode ω (q) is

$$\omega s(q) = cs\,q. \qquad (2)$$

However, this model is a gross approximation and fails completely to consider or describe optical modes [10-12]. The next step in the modeling of lattice dynamics was a series of phenomenological force models which built on each previous model, and the development of a few ab initio models as well. The latter of these methods, the ab

initio models, were created in the 1970's and require an accurate and parameter less calculation of microscopic electron response to lattice vibrations [13-17]. These calculations can be done via a number of different techniques such as the Frozen phonon method and the Planar force constant method. However, ab initio calculations of lattice dynamics of nanostructures have only recently become feasible and these are still limited to the smallest and thinnest of structures with only a few atoms in the unit cell. This is due to the lack of translation symmetry in one or more directions which introduces difficulties in modeling the periodic potentials of the crystal structure. In particular, nanowires present a very difficult problem as calculations of the phonon dispersion relations for structures with greater than 100 atoms become nearly impossible within current computational limits [11,14-18]. This has led to the use of phenomenological models for modeling nanostructures. These were first developed in 1914 and have been continuously improved and adapted for more advanced structures up until the present day.

1.2 Adiabatic Bond Charge Model (BMC)

The adiabatic bond charge (BMC) method was originally developed by Weber in 1976 for studying the lattice dynamics of tetrahedral bonded bulk group-IV semiconductors such as silicon and diamond [2-3,19-24]. The model was also adapted by Rustagi and Weber for studying III-V semiconductors such as Gallium Arsenide. In Weber's approach, the atom is considered a non-polarizable ion core and a shell of valence electrons. The valence charge density is considered as point charges, called bond charges (bc's), which are located midway (in the IV-IV case) along the tetrahedral bonds between the nearest homopolar neighbors as illustrated in Fig. (1)

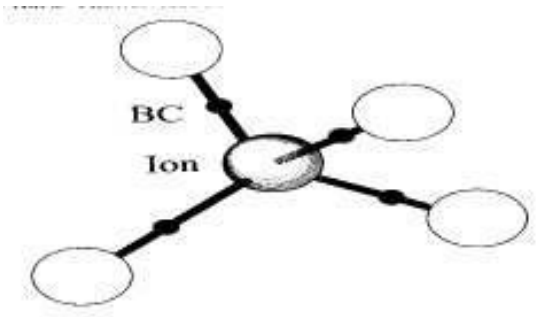

Fig- 1: A schematic illustrating the concept of bond charges and ions in the adiabatic bond charge model [25].

These bond charges are allowed to move adiabatically and are assumed to have zero mass. The equations of motion for the ions and their bond charges are evaluated and a dynamical matrix is obtained by considering three types of interaction: (i) Coulomb interaction between all particles within the structure (ion-ion, ion-bc, bc-

bc), which is evaluated using the Ewald summation technique, (ii) short range central force interaction acting centrally between nearest neighbors (ion-ion, ion-bc, bc-bc), and (iii) a rotationally invariant Keating type bond bending interaction, depending on the bc-ion-bc angle. Once these interactions are taken into account, dispersion relations of the form ω = ω (qs) are obtained for the lattice dynamics of the system. To calculate the phonon dispersion relations, one must understand how the dynamical matrix is constructed and how it is made of these three force components (Coulombic, central, and Keating-type). In the results of calculations for silicon bulk are shown. As can be seen, these figure. The phonon dispersion curves for bulk silicon. The experimental results of Dolling and Nilsson are shown in the dark and light diamonds respectively. Fig. (2)

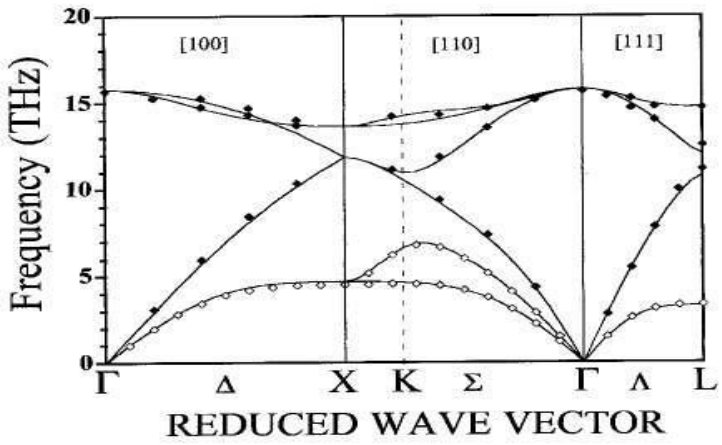

Fig- 2: The phonon dispersion curves for bulk silicon. The experimental results of Dolling [117 and Nilsson [118] are shown in the dark and light diamonds respectively [26].

1.3 The C-Matrix

To create a dynamical matrix, one normally begins with the classical equations of motion for the atoms within the crystal structure in terms of the interatomic potential and the atomic displacements. It can be seen from Eq. that the classical equation of motion may be written as:

$$M_b \frac{d^2 u_i(lb)}{dt^2} = -\sum_{l'b'} \Phi_{ij}(lb, l'b')\, u_j(l'b'), \qquad (3)$$

where Mb is the mass of the atom in the unit cell, t is the time co-ordinate and the other symbols have their usual meanings. To evaluate Eq., a trial solution is applied. It is of the form

$$u_i(lb) = \frac{1}{\sqrt{M_b}} \sum_q U_i(q;b) \exp[i(q.x(lb)-\omega t)], \quad (4)$$

where Ui (q;b) is the amplitude of vibration of the b_{th} atom in the unit cell and a function of the wave-vector q. By applying this relation, Eq. becomes

$$\omega^2 e_i(b;qs) = \sum_{b'j} C_{ij}(bb'|q) e_j(b';qs), \quad (5)$$

Where the C matrix has 3N eigensolutions with eigenvalues ω2 (qs) and eigenvectors e(b;qs) and N is the number of atoms per unit cell. The eigenvectors describe the oscillations of the atoms for each vibration mode and ω(qs) has its usual meaning. The C matrix is related to the force constant matrix,Φ, by

$$C_{ij}(bb'|q) = \frac{1}{\sqrt{M_b M_{b'}}} \sum_1 \Phi i_j(ob;lb) \exp[-iq.(x(0b)-x(lb))]. \quad (6)$$

1.3.1 C-Matrix in the BCM

In the adiabatic bond charge model, the equations of motion are set up in the same manner as previously, but one must now consider the bond charges as additional particles in the system [27]. These bond charges are positioned midway between each pair of adjacent ions as shown in fig. Hence Eq. becomes extended as

$$M_{\omega^2} e_{ion} = C_{ion\text{-}ion}\, e_{ion} + C_{ion\text{-}bc}\, e_{bc}, \quad (7)$$

And

$$M'_{bc}\omega^2 e_{bc} = C_{bc\text{-}ion} e_{ion} + C_{bc\text{-}bc} e_{bc}, \quad (8)$$

where M is the ion mass matrix, M'bc is the bond charge mass matrix and eion and ebc are eigenvectors of the two coupled dynamical equations for ion and bond charge displacement. As mentioned earlier, this is simplified bythe adiabatic assumption that M'bc =0 for all the bond charges. Hence the bond charge eigenvector may be eliminated from Eq. (7) by applying Eq. (8) Therefore, the effective equation of motion becomes

$$M\omega^2 e_{ion} = [C_{ion\text{-}ion} - C_{ion\text{-}bc} C^{-1}_{bc\text{-}bc} C_{bc\text{-}ion}] e_{ion}, \quad (9)$$

To solve Eq. (9) each of these matrices can be evaluated in terms of Columbic and non-columbic components. The repulsive Columbic force can be summarized by the force constant matrix

$$\varphi^C_{ij}(lb;l'b') = \frac{n_c Z^2}{e} \frac{1}{4\pi\varepsilon_0} \frac{\delta^2}{\delta x_i \delta x_j} \frac{Q_b Q_{b'}}{r}\Big|_{r = x(lb;\, l'\, b')'} \quad (10)$$

with the condition that (lb) ≠ (l'b'). Here, ε0 is the permittivity of free space, Qb and Qb' are the charge of the bth and b' th atoms respectively, r is the distance between these two atoms, nC is the product of the charges of the ion and the bond charges depending on the interaction (so ion-ion = 4, bc-bc=1 and ion-bc=2) and zε2 is an adjustable parameter.

3 Results

3.1 Standalone nanowires

Phonon dispersion curves were calculated for standalone silicon nanowire of cross-section d x d, with d ranging from 0.543 nm (viz. d=a, the bulk lattice constant) up to 3.801 nm (viz. d = 7a). In general, two important features were noted in the dispersion curves and density of states curves: folding effects; i.e. bulk results folded on to the nanowire Brillouin zone and confinement effects; i.e. phonon modes which arise due to reduced dimensionality upon the formation of wires. As can be observed in Fig., the ultrathin nanowire (the thinnest considered 0.543 nm x 0.543 nm) shows several unusual and unique properties not seen in thicker nanowires. All the non-acoustic modes are almost flat and dispersion less, even in the direction of propagation, Γ-Z. The acoustic modes have very high group

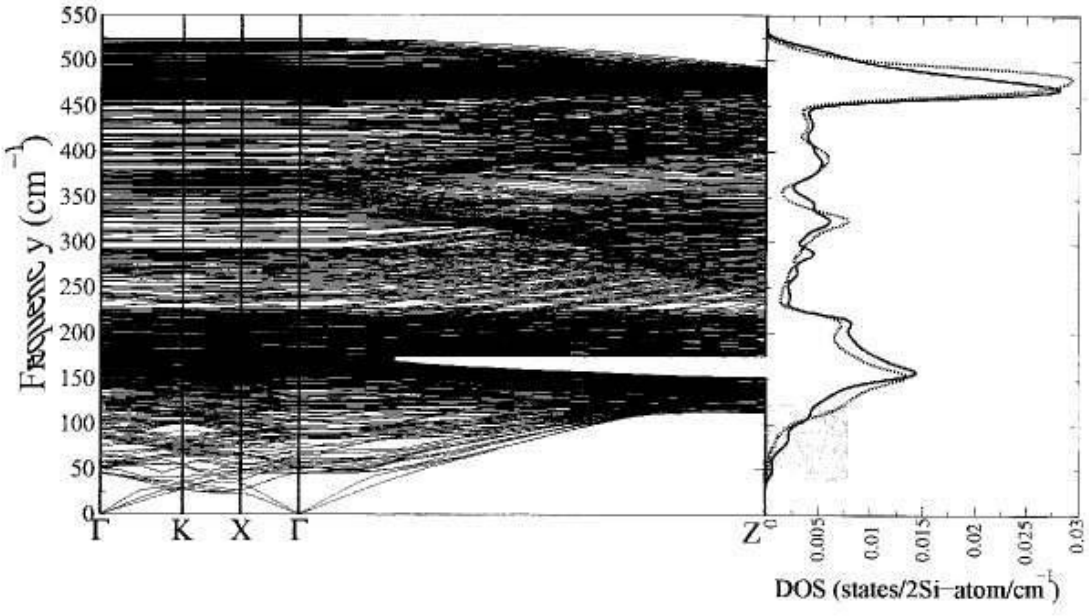

Figure 3: The phonon dispersion curves and density of states for a silicon nanowire of cross section 3.8 nm x 3.8 nm. Also shown are the density of states for the wire (hold line) and the density of states of bulk silicon (dashed

line). Velocities near the zone center in the Γ-Z direction, nearly three times greater than the corresponding velocities in bulk silicon. Another feature of note is the appearance of several gaps in the density of states. These gaps are located both within and above the bulk silicon acoustic range as shown in Fig3.

Figure 4: The amplitude of atomic vibration of the three lowest non-zero modes very near the zone-center for a nanowire of cross section 3.8 nm x 3.8 nm.

The darker the atom, the higher its relative amplitude of vibration compared to other atoms: (a) lowest non-zero mode, (b) second lowest non-zero mode, (e) third lowest non-zero mode as shown in Fig. 4.

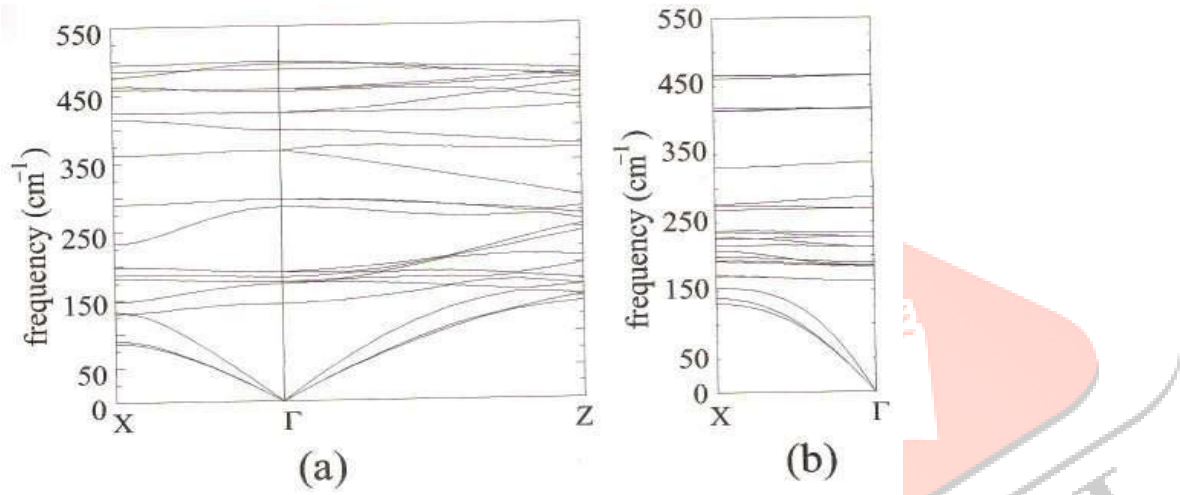

Figure 5: The phonon dispersion curves for: (a) a silicon nanoslab of thickness 0.543 nm; (b) a silicon nanodot of size 0.543 nm x 0.543 nm x 0.543 nm.

In all three directions and, as such, provide no direction of propagation. indeed for silicon Nano dots the phonon dispersion curves are flat and dispersion less in all directions for all sizes considered here (up to d = 3a = 1.68 nm in width), as shown in Fig. 5 (b). This is similar to what is observed in the directions of confinement for nanowires. In the thinnest silicon Nano slab the phonon branches are flat and dispersion less in the direction of confinement, though not to the same degree as for the thinnest nanowire, as shown in Fig. 5 (a). As the size of confinement d increases it can be seen that the Nano dots shown much greater flatness in their branches than a nanowire of the same size of confinement. This is not unexpected as there is no direction of propagation for the Nano dot, and thus quantization effects completely dominate. Phonon branches remain rather flat for slab thickness d =2a = 1.08 nm and begin to exhibit dispersive behavior, for thicker slabs. However, unlike the ultrathin nanowire or ultra-small Nano dot, the ultrathin Nano slab does not show flatness in the direction of propagation for many of

its branches. This is a direct result of a Nano slab only having one degree of confinement as opposed to the nanowires with two degrees of confinement. Thicker Nano slabs show much less flatness in their branches, even in the direction of confinement as size increases.

Table1: The zone-center lowest non-zero mode for different sizes and dimensionality of nanostructure.

Dimensionality	Size of confinement, d(nm)	ωσ(cm-1)
2	1.68	84.46
2	1.09	108.84
2	0.54	143.69
1	1.68	80.21
1	1.09	103.46
1	0.54	158.22
0	1.68	91.20
0	1.09	119.94
0	0.54	163.29

4. Summary and results:

Silicon nanostructures have several common features in their lattice dynamics. It can be seen for the ultra-small case of each structure that all branches except the acoustic are flat and dispersion less regardless of whether the system is zero-, one-or two-dimensional. As the size of these structures increases, these branches are seen to become dispersive in the direction of propagation. Eventually, as size increases, the branches in the direction of confinement start to follow a similar trend. In all systems studies, the characteristic lowest non-zero zone center mode with frequency $\omega\sigma$ is calculated and shown to decrease with the size of the nanostructure. An analytic fit has been presented for the size variation of this mode for simple structures of Nano dots, nanowires and Nano slabs. It is also observed that in all systems the highest optical mode is lowered and for simple systems this behavior can be explained using a simple diatomic model. The calculated results for such variation have been fitted to analytic expression. These trends are also observed in the case of nanowires deposited on substrates. For this system the phonon dispersion is in general dominated by the substrate. In particular, the phonon branches in the Γ - Y direction become more dispersive than in the stand alone nanowire, showing that the addition of the slab reduces quantization in that plane. Also, the frequency $\omega\sigma$ of a nanowire deposited upon a substrate is lower than that of either of the two stand alone systems. All these silicon nanostructures shows several interesting and important vibrational features. In the next section the lattice dynamics of carbon nanotubes are introduced. As can be seen, these structures have several features in common as well as some features which are different. The lattice dynamics of carbon nanotubes show several interesting features. Some of these features are common with silicon nanostructures and some are not. For nanotubes, the lattice dynamics have been well studied on an atomistic level. In this section a review of the history and development of these novel and interesting structures is presented. A continuum model based upon research by Mahan and Zhang et al. is modified and presented. Results from this model are compared and contrasted with silicon nanostructures. These are make extensive use of the phonon dispersion relations derived in the following sections to derive and calculate the thermal properties of carbon nanotubes.

5. Conclusion

Nanostructures have several common features in their lattice dynamics. All structures show the appearance of low energy optical branches in their phonon dispersion curves, the branch associated with ωσ in the silicon nanostructures and the carbon nanotube as well as the additional branch associated with ωB in the carbon nanotube. Also, all of the thinnest structures have high zone-center group velocity for their acoustic phonon branches, when compared to either bulk or larger nanostructures. For the silicon nanostructures, it can be seen for the ultra-small case of each structure that all branches except the acoustic are flat and dispersion less regardless of whether the system is zero-, one-or two-dimensional. Conversely, the continuum model of the nanotube shows that the group velocity of the low optical modes is much large for $k > 1$. As the size of the silicon structures increases, these branches are seen to become dispersive in the direction of propagation like the nanotube. In all the materials studied here, the characteristic lowest non-zero zone center mode with frequency ωσ is calculated and shown to decrease with size of the nanostructure as $\omega\sigma \alpha 1/ra$ where α depends on the type of nanostructure. An analytic fit has been presented for the size variation of this mode for the silicon nanostructures (dots, wires and slabs) and the behavior of low-lying modes in carbon nanotubes is explained from theory. For the silicon systems considered, it is observed that the highest optical mode is lowered when compared with bulk and this behavior can be predicted.

References

[1] L. Evans and P. Bryant, LHC Machine, JINST 3 (2008) S08001.

[2] R. Assmann, M. Lamont and S. Myers, A brief history of the LEP collider, Nucl. Phys. Proc. Suppl. 109B (2002) 17–31.

[3] The CERN accelerator complex. te-epc-lpc.web.cern.ch/te-epc-lpc/ machines/pagesources/Cern-Accelerator-Complex.jpg.

[4] A. A. Glazkov et al., Duoplasmatron-type ion source with improved technical and operational performance for linear accelerator, Proceedings of the 3. European particle accelerator conference 1 (1992) 993–995.

[5] ATLAS Collaboration, The ATLAS Experiment at the CERN Large Hadron Collider, JINST 3 (2008) S08003.

[6] CMS Collaboration, The CMS experiment at the CERN LHC, JINST 3 (2008) S08004.

[7] ALICE Collaboration (K. Aamodt et al.), The ALICE experiment at the CERN LHC, JINST 3 (2008) S08002.

[8] LHCb Collaboration (A. Alves et al.), The LHCb Detector at the LHC, JINST 3 (2008) S08005. [9] J. L. Pinfold, The MoEDAL Experiment at the LHC, EPJ Web Conf. 71 (2014) 00111.

[10] LHCf Collaboration (0. Adriani et al.), The LHCf detector at the CERN Large Hadron Collider, JINST 3 (2008) S08006.

[11] TOTEM Collaboration (G. Anelli et al.), The TOTEM experiment at the CERN Large Hadron Collider, JINST 3 (2008) S08007.

[12] F. Bordry et al., The First Long Shutdown (LS1) for the LHC, MOZB202 (2013). 141 142 Bibliography

[13] CDF Collaboration (R. Blair et al.), The CDF-II detector: Technical design report, FERMILAB-DESIGN-1996-01, FERMILAB-PUB-96-390-E (1996).

[14] T. Varol, Muon Performance in the Presence of High Pile-up in ATLAS, arXiv:1212.0392 [hep-ex].

[15] ATLAS Experiment Luminosity Public Results. twiki.cern.ch/twiki/bin/view/AtlasPublic/LuminosityPublicResults.

[16] ATLAS Collaboration, ATLAS pixel detector: Technical Design Report, CERN-LHCC-98-013, ATLAS-TDR-11 (1998).

[17] ATLAS Collaboration, ATLAS pixel detector electronics and sensors, JINST 3 (2008) P07007.

[18] ATLAS Collaboration, ATLAS Insertable B-Layer Technical Design Report, CERN-LHCC-2010-013, ATLAS-TDR-19 (2010).

[19] B. Dolgoshein, Transition radiation detectors, Nucl. Instrum. Meth. A326 (1993) 434–469. [20] ATLAS Collaboration, ATLAS muon spectrometer: Technical design report, CERN-LHCC-97-22, ATLAS-TDR-10 (1997).

[21] ATLAS Collaboration, Performance of the ATLAS Trigger System in 2010, Eur. Phys. J. C72 (2012) 1849, arXiv:1110.1530 [hep-ex].

[22] ATLAS Collaboration, ATLAS first level trigger: Technical design report, CERN-LHCC-98-14, ATLAS-TDR-12 (1998).

[23] ATLAS Collaboration, ATLAS high-level trigger, data acquisition and controls: Technical design report, CERN-LHCC-2003-022, ATLAS-TRD-016 (2003).

[24] ATLAS Collaboration, ATLAS: Detector and physics performance technical design report. Volume 1, CERN-LHCC-99-14, ATLAS-TDR-14 (1999).

[25] ATLAS Collaboration, Improved luminosity determination in pp collisions at √ s = 7 TeV using the ATLAS detector at the LHC, Eur. Phys. J. C73 (2013) 2518, arXiv:1302.4393 [hep-ex]. [26] ATLAS Collaboration, ATLAS Forward Detectors for Measurement of Elastic Scattering and Luminosity, Tech. Rep. CERN-LHCC-2008-004, ATLAS-TDR-18, 2008.

[27] ATLAS Collaboration, The ATLAS Simulation Infrastructure, Eur. Phys. J. C70 (2010) 823–874, arXiv:1005.4568 [physics.ins-det].